Icarus 306 (2018) 16–24

Contents lists available at ScienceDirect

Icarus

journal homepage: www.elsevier.com/locate/icarus

Near surface bulk density estimates of NEAs from radar observations and permittivity measurements of powdered geologic material

Dylan Hickson[a], Alexandre Boivin[b], Michael G. Daly[a,*], Rebecca Ghent[b,c], Michael C. Nolan[d], Kimberly Tait[e], Alister Cunje[b], Chun An Tsai[b]

[a] Centre for Research in Earth and Space Science, York University, Toronto, Canada
[b] Solar System Exploration Group, Department of Earth Sciences, University of Toronto, Toronto, Canada
[c] Planetary Science Institute, Tucson, USA
[d] Lunar and Planetary Laboratory, University of Arizona, Tucson, USA
[e] Department of Natural History, Mineralogy, The Royal Ontario Museum, Toronto, Canada

ARTICLE INFO

Article history:
Received 15 September 2017
Revised 9 January 2018
Accepted 17 January 2018
Available online 2 February 2018

Keywords:
Asteroids
surfaces
Asteroid Bennu
Radar observations
Regoliths

ABSTRACT

The variations in near-surface properties and regolith structure of asteroids are currently not well constrained by remote sensing techniques. Radar is a useful tool for such determinations of Near-Earth Asteroids (NEAs) as the power of the reflected signal from the surface is dependent on the bulk density, ρ_{bd}, and dielectric permittivity. In this study, high precision complex permittivity measurements of powdered aluminum oxide and dunite samples are used to characterize the change in the real part of the permittivity with the bulk density of the sample. In this work, we use silica aerogel for the first time to increase the void space in the samples (and decrease the bulk density) without significantly altering the electrical properties. We fit various mixing equations to the experimental results. The Looyenga–Landau–Lifshitz mixing formula has the best fit and the Lichtenecker mixing formula, which is typically used to approximate planetary regolith, does not model the results well. We find that the Looyenga–Landau–Lifshitz formula adequately matches Lunar regolith permittivity measurements, and we incorporate it into an existing model for obtaining asteroid regolith bulk density from radar returns which is then used to estimate the bulk density in the near surface of NEA's (101955) Bennu and (25143) Itokawa. Constraints on the material properties appropriate for either asteroid give average estimates of $\rho_{bd} = 1.27 \pm 0.33$ g/cm^3 for Bennu and $\rho_{bd} = 1.68 \pm 0.53$ g/cm^3 for Itokawa. We conclude that our data suggest that the Looyenga-Landau-Lifshitz mixing model, in tandem with an appropriate radar scattering model, is the best method for estimating bulk densities of regoliths from radar observations of airless bodies.

1. Introduction

Asteroids are of significant interest in planetary science as they are generally acknowledged as being relatively unaltered material left over from the formation of the solar system. At present there are two space missions aimed at returning regolith samples from C- group carbonaceous asteroids to better understand these primitive objects. NASA's Origins, Spectral Interpretation, Resource Identification, Security, Regolith Explorer (OSIRIS-REx) mission is scheduled to arrive at Near-Earth asteroid (NEA) (101955) Bennu, a B- type asteroid according to the Bus-DeMeo taxonomy, in 2019 for analysis and sample acquisition (Lauretta et al., 2017, 2015; Clark et al., 2011; DeMeo et al., 2009). JAXA's Hayabusa2 mission is targeting (162173) Ryugu, a Cg- type NEA according to the SMASSII taxonomy, for analysis and sample acquisition and is scheduled to arrive at the asteroid in 2018 (Yoshikawa et al., 2014; Binzel et al., 2001; Bus and Binzel, 2002). A previous asteroid sample return mission, JAXA's Hayabusa, rendezvoused with (25143) Itokawa, an S- type chondritic asteroid, in 2005 and returned small grains of regolith for analysis in 2010 (Yoshikawa et al., 2015). Collective constraints on the NEA and main belt asteroid (MBA) populations suggest that for most asteroids total bulk density is significantly lower than supposed grain densities, indicating substantial porosity (Britt et al., 2002). Remote sensing of asteroids is necessary to constrain their densities for science objectives and to provide engineering constraints for current and future space missions.

1.1. Asteroid radar astronomy

Planetary radar has been widely used to survey and characterize numerous NEAs as well as some MBAs (Benner et al., 2015). Re-

* Corresponding author.
E-mail address: dalym@yorku.ca (M.G. Daly).

https://doi.org/10.1016/j.icarus.2018.01.018
0019-1035/

flections contain information about the near-surface regolith material of the target asteroid within the penetration depth of the radar signal, typically on the scale of a few metres (Campbell, 2016; Harmon et al., 2004). Modern radar systems such as the Arecibo Observatory and Goldstone Solar System Radar that are used to observe asteroids make use of polarimetry, in which a circularly polarized radar beam is transmitted towards a target and the power and polarization of the returned radar echo is measured. Polarized radar echoes received in the same sense as that transmitted are termed SC and are indicative of multiple and diffuse scattering caused by surface roughness and embedded rocks in the regolith on the scale of the incident wavelength (Ostro et al., 1985; Harmon et al., 2004). Specular reflections from smooth (on the scale of the observing wavelength) surfaces will reverse the handedness of an incident radar signal and cause the reflection to be received in the opposite sense to that transmitted, termed OC (Ostro et al., 1985; Carter et al., 2011). The radar cross section, σ, of a given asteroid is defined by the radar equation for a given receiving mode polarization (Ostro, 1993):

$$P_{rcv} = \frac{P_{tx} G_{ant}^2 \lambda^2 \sigma}{(4\pi)^3 r^4}. \quad (1)$$

The radar cross section σ can be converted into the geometric radar albedo, $\hat{\sigma} = \frac{\sigma}{A_p}$, if the apparent projected area A_p is known. The circular polarization ratio is defined as $\mu_c = \frac{\sigma_{SC}}{\sigma_{OC}}$, and is an indication of the surface roughness on wavelength scales. With the assumption of an appropriate radar scattering law, the Fresnel reflectivity of the material within the penetration depth of the radar signal can be calculated from the OC geometric radar albedo, e.g. (Mitchell et al., 1996; Ostro et al., 1985). For targets with low surface roughness (and hence low μ_c) the dominant scattering mechanism is specular reflection, making this approximation valid. The Fresnel reflectivity is dependent on the index of refraction of the regolith which is driven by the relative (to vacuum) complex permittivity, $\tilde{\epsilon_r} = \epsilon_r^{'} + i\epsilon_r^{''}$ of the material, assuming a magnetic permeability equal to unity. The real part of the relative complex permittivity, $\epsilon_r^{'}$, will be referred to as the dielectric constant for the remainder of this paper, and is proportional to the stored electrical energy in a material, controlling its reflectivity. The imaginary part of the relative complex permittivity, $\epsilon_r^{''}$, is related to the energy loss with wave propagation in a material. The loss tangent, $tan(\delta) = \frac{\epsilon^{''}}{\epsilon^{'}}$, is the ratio of the imaginary part to the real part of the relative complex permittivity and is an indication of how significant energy loss is in a material. For asteroid regolith with low metal content (and magnetic permeability equal to unity, or one) the Fresnel reflectivity is determined by the dielectric constant. Therefore the effective dielectric constant relating to all of the material making up the near surface regolith on an asteroid can be indirectly measured using radar. An understanding of how the dielectric constant of regolith constituents, essentially powdered rock, changes with environmental properties would allow such properties to be interpolated from radar data. One property, the bulk density of a material, has been shown to have a strong correlation with the dielectric constant (Campbell and Ulrichs, 1969; Olhoeft and Strangway, 1975; Ulaby et al., 1990).

1.2. Inversion of dielectric constant for bulk density

Electromagnetic mixing equations have been used extensively in many areas of research to solve for the dielectric properties of a wide range of composite materials and geometries (Sihvola, 1999). Porous regolith can be treated as a composite material comprised of solid particle grains and void space (vacuum). In order for homogenization of the dielectric properties to be valid for a mixture, the scale of the dielectric heterogeneity must be smaller than the wavelength of the incident electric field. This requirement is usually satisfied for planetary radar as Lunar and asteroidal regolith grain sizes are generally in the range of 30–800 μm and are much smaller than S- and X- band radar (λ = 12.6 cm, 3.5 cm) wavelengths typically used for asteroid surveys, though the unusual scattering properties of E- and V- type asteroids could be the result of large grains (Benner et al., 2015; Clark et al., 2002; McKay et al., 1991; Benner et al., 2008). In the field of planetary science there have been several attempts to use mixing equations to extract meaningful surficial interpretations from planetary radar reflections. Campbell and Ulrichs (1969) investigated the electrical properties of terrestrial rocks, minerals, and several meteorites in order to constrain radar investigations of the Lunar regolith. They found that the Rayleigh mixing formula (also referred to as Maxwell-Garnett) provided the best fit for the measured dielectric constant of powdered rock samples at varying densities. In another study, Olhoeft and Strangway (1975) compiled 92 measurements of the complex permittivity of Lunar regolith samples returned from NASA's Apollo missions. They found that the dielectric constant varied with rock bulk density and the loss tangent was dependent on both density and iron oxide and titanium dioxide concentrations. They fitted the dielectric constant data with a power law of the form:

$$\epsilon_{eff} = a^{\rho_{bd}}. \quad (2)$$

Here, ϵ_{eff} is the effective dielectric constant of the regolith sample, a is a constant, and ρ_{bd} is the bulk density of the regolith sample. Olhoeft and Strangway (1975) showed that Eq. (2) is identical to the Lichtenecker mixing equation (Lichtenecker, 1926):

$$log(\epsilon_{eff}) = \sum_i f_i log(\epsilon_i) \quad (3)$$

Here, f_i is the volume fraction of the ith component of a mixture and ϵ_i is the dielectric constant of the ith component. Eq. (2) is equivalent to Eq. (3) for a two phase mixture approximating planetary regolith with one component constrained as vacuum ($\epsilon_{vacuum} = 1$) and $a = \epsilon_s^{1/\rho_s}$, where ϵ_s is the dielectric constant of the solid rock grains and ρ_s is the solid density, or particle density, of the solid rock grains. The regression of the 92 Lunar regolith dielectric constant measurements by Olhoeft and Strangway (1975) resulted in the expression: $\epsilon_{eff} = (1.93 \pm 0.17)^{\rho_{bd}}$, which corresponds to a solid rock grain dielectric constant of ϵ_s = 7.7 and a particle density of $\rho_s = 3.1\,g/cm^3$. These values are in agreement with accepted values in the literature for average Lunar regolith properties (Carrier et al., 1991).

Eq. (2) has been used by several authors in the years following its introduction by Olhoeft and Strangway (1975) for planetary radar applications; however, the value for the constant, a, varies (Table 1). The studies shown in Table 1 derived a value for a from statistical regression analysis of dielectric measurements of a variety of Lunar regolith samples and terrestrial rocks. In the context of the Lichtenecker formula, the variation in a in Table 1 implies that the physical properties ϵ_s and ρ_s must vary across the samples used for the dielectric measurements referenced in these

Table 1
Values of a found in the literature. *excluding temperature dependence term.

Reference	Form of Eq. (2)
Olhoeft and Strangway (1975)	$\epsilon_{eff} = 1.93^{\rho_{bd}}$
Bussey (1979)	$\epsilon_{eff} = 2.10^{\rho_{bd}}$
Garvin et al. (1985)	$\epsilon_{eff} = 1.87^{\rho_{bd}}$
Ulaby et al. (1990)	$\epsilon_{eff} = 1.96^{\rho_{bd}}$
Carrier et al. (1991)	$\epsilon_{eff} = 1.92^{\rho_{bd}}$
Campbell (2002)	$\epsilon_{eff} = 1.96^{\rho_{bd}}$
Barmatz et al. (2012)	$\epsilon_{eff} = 2.15^{\rho_{bd}}$
Palmer et al. (2015)*	$\epsilon_{eff} = 1.85^{\rho_{bd}}$

studies. In general, the theoretical connection of Eq. (2) to the material properties of the samples used in these studies is not addressed, and the value for a is found empirically. The empirically derived value of a is not cross checked with the theoretical value of a that would correspond to the appropriate values of ϵ_s and ρ_s for a given sample.

In this study measurements of the dielectric constant of powdered geologic material over a range of bulk densities are used to compare the corresponding fits for various mixing equations. The validity of the Maxwell-Garnett and Lichtenecker mixing equations, which are predominantly used in the literature for planetary radar inversion, is investigated. The best fit mixing equation is then incorporated for use in an existing model aimed at estimating asteroid near surface bulk density from radar data.

2. Experimental methods

2.1. Instrumentation

Powdered rock samples are measured in a 14 mm diameter GR 900-LZ (15 cm length) coaxial airline connected to a Keysight E5071C ENA series vector network analyzer (VNA). The GR-900-LZ coaxial airline operates up to 8.5 GHz; however, the phase uncertainty in the VNA makes data collected below roughly 500 MHz unusable. The uncertainty in the scattering parameters is calculated from the network analyzer using METAS VNA Tools II software (Wollensack et al., 2012). To keep uncertainty to a minimum, only data above 1 GHz is used in this study. A full two-port Through-Reflect-Match (TRM) calibration of the network analyzer is completed before all measurements to reduce systematic errors (Rytting, 2001; KeysightTechnologies, 2014). The complex permittivity of powdered samples is calculated from the average scattering parameters (average of forward S_{11}, S_{21} and backward S_{22}, S_{12}) measured by the VNA using the non-iterative algorithm outlined in Boughriet et al. (1997).

We designed and built a custom environment chamber to isolate the filled coaxial airline from atmospheric humidity and temperature fluctuations during the measurement process. The pressure in the chamber was reduced from atmospheric pressure ($\approx$760 Torr) down to $\approx$950 mTorr for 30–60 min prior to all measurements. The purpose of maintaining the low pressure measurement environment is to resist adsorption of water onto rock grains. As water has a high dielectric constant, any adsorbed water will increase the measured permittivity and decrease the validity of a two phase (solid rock grains and air) mixing approximation.

2.2. Sample characterization and preparation

The geologic samples used in this study consist of aluminum oxide (Al_2O_3) and a dunite. The dielectric constant of aluminum oxide is well characterized (e.g. (Hickson et al., 2017; von Hippel, 1954; Gershon et al., 2001; Rajab et al., 2008; Tuhkala et al., 2013)) and the sample consists of a single mineral, removing the variability of composition from permittivity measurements and subsequent modeling. The aluminum oxide was supplied in powdered form by Kramer Industries, Inc. in 76 µm and 102 µm average grain size sample batches with a manufacturer specified particle density $\rho_s = 3.8\,\mathrm{g/cm^3}$. The dunite sample was pulverized into powder form using an aluminum oxide ceramic mortar and pestle in two batches to average grain sizes of 113 µm and 109 µm. X-ray diffraction (XRD) and Raman analysis were performed at the Royal Ontario Museum to constrain the composition of the dunite sample to be roughly 95% nearly pure forsterite (CrystalSleuth, RRUFF ID R060539) (Mg1.849:FeO0.151, PDF 01-080-1639). The Raman system used was a Horiba LabRAM utilizing a 532 nm laser with a 1300 nm spot size. The XRD system used was a Bruker D8 Advance with a Cu source operating at 40 kV and 40 mA with a Linxeye detector. The XRD system is equipped with a twin primary motorized slit of 0.6 mm, a Ni filter, and a twin secondary motorized slit of 5.5 mm. The particle density of the dunite sample was measured in laboratory by measuring the mass of displaced water when immersed in distilled water, and was found to be $\rho_s = 3.29 \pm 0.06\,\mathrm{g/cm^3}$. All powdered samples were oven baked at a constant temperature of 250°C for at least 12 h prior to measurement to evaporate residual moisture.

2.3. Density variation using silica aerogel

To achieve high accuracy permittivity measurements of powdered samples, the sample must be distributed homogeneously throughout the coaxial airline. Uniform particle packing density was established in the airline for each measurement using a custom airline filling fixture that vibrates the airline during the filling process. It was observed that the filling procedure produces a bulk density that reaches an asymptotic limit after a given vibration time. Vibrating the airline throughout the filling process produces nearly uniform porosity along the airline's length. As a result of this, for a given particle size distribution there are only slight variations in the powder's bulk density for repeated measurements of the same sample. In order to vary the bulk density of the powdered aluminum oxide and dunite samples in the airline we developed a novel approach that utilizes silica aerogel particles. Silica aerogel is a highly porous, low dielectric constant material that is composed of mostly void space (Dorcheh and Abbasi, 2008; Gurav et al., 2010). Hrubesh and Pekala (1994) measured the dielectric constant of silica aerogel and found the gas phase to dominate the measurements and the dielectric constant varied linearly with density. The Enova IC3100 silica aerogel particles used in this study are supplied by Cabot Corporation in the particle size range of 2–40 µm with a particle density of $\rho_s = 0.12 - 0.15\,\mathrm{g/cm^3}$ and hydrophobic surface chemistry. By incrementally adding silica aerogel particles to the powdered aluminum oxide and dunite samples we are able to increase the void space, and hence lower the bulk density, without significantly altering the dielectric constant of the mixture from that of a mixture with vacuum voids. The silica aerogel/sample mixture was made homogeneous by mechanical mixing for all samples. Fig. 1 shows the powdered dunite sample combined with silica aerogel before and after mixing the two materials.

The dielectric constant of the silica aerogel particle phase in the mixture can be calculated from the Hrubesh and Pekala (1994) model. For the particle densities mentioned above, the dielectric constant is $\epsilon_s < 1.2$. By mass this phase is insignificant in the sample mixture and at the highest volumetric proportion of silica aerogel used in this study the dielectric constant calculated from the Hrubesh and Pekala (1994) model is $\epsilon_s < 1.042$, and therefore its contribution to the measured effective permittivity is treated the same as void spaces. With respect to the modeling results that are presented in Section 4.2, when calculating the dielectric constant of the solid rock grains the difference between considering the silica aerogel phase in the mixing models and treating the phase as voids is $\epsilon_s < 0.02$, or less than a 0.6% difference. To our knowledge this is the first time that silica aerogel particles have been used to alter the bulk density of a powder for material measurements.

3. Measurement results

A typical measurement of the dielectric constant for powdered samples in this study is shown in Fig. 2. The dielectric constant of the dunite sample is non-dispersive (frequency independent)

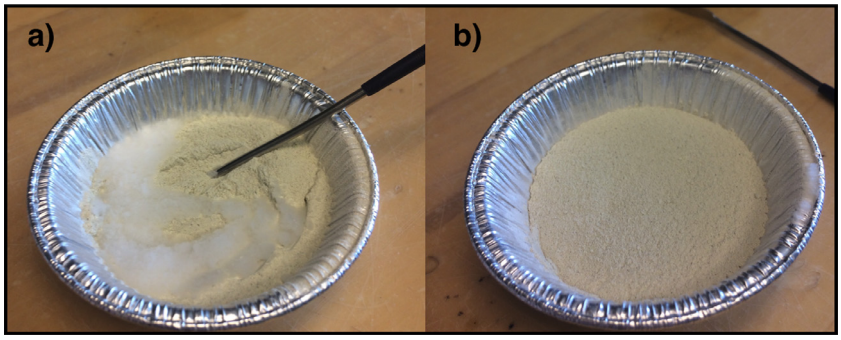

Fig. 1. a) Powdered dunite with silica aerogel prior to mixing b) Resulting dunite/silica aerogel mixture.

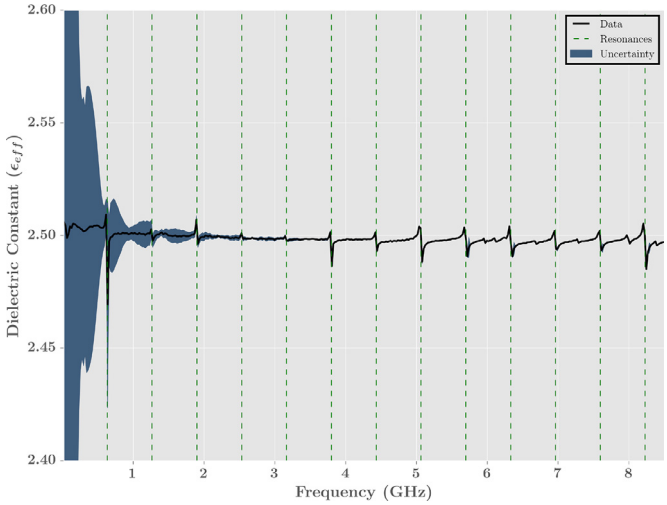

Fig. 2. Broadband measurement of the dielectric constant of a dunite/silica aerogel sample used in this study.

over the frequencies measured. Similar results are observed for the aluminum oxide samples. The dotted green lines in Fig. 2 correspond to half-wavelength resonances due to phase uncertainty (e.g. Boughriet et al., 1997). We take an average of measured values at midpoints between resonance peaks as the dielectric constant for each measurement. By doing so we exclude the contribution of the resonance peaks while reporting a value for the dielectric constant consistent over the frequencies measured. The mid point between the first two resonance peaks was excluded from the averaging due to the large uncertainty. Although the complex permittivity was measured for each sample, the subsequent modeling is focused on the dielectric constant data as the loss tangent is not the dominant part of the permittivity in determining radar reflectivity from asteroid regolith with low metal content. The bulk density of the sample for a given measurement was calculated from the mass of the sample and the known volume of the coaxial airline. A summary of the aluminum oxide and dunite powder sample measurements is given in Table 2. The error in the dielectric constant reported in Table 2 is the sum of the standard deviation between the averaged measurement points and the propagated uncertainty in the calculation of the dielectric constant for each point. The error is higher for the aluminum oxide measurements since these samples showed slightly more dispersion than the dunite samples. The error in the bulk density is derived from the propagation of the measurement error in measuring the sample mass (± 0.7 mg), length (± 0.01 mm) and diameter (± 0.0025 mm) of the coaxial airline.

4. Mixing equation modeling

4.1. Mixing formulas

The common aspect of all electromagnetic mixing equations is that the effective dielectric constant of a mixture is a function of the dielectric constants of the mixture components and their respective volume fractions. For the powder measurements presented in Table 2, the mixture comprises two components: solid rock/mineral grains and air (as mentioned in Section 2.3, the silica aerogel phase is treated as voids, or air). The volume fraction of air is equivalent to the porosity, ϕ, of the sample and can be calculated from the bulk density, ρ_{bd}, and the solid density, ρ_s, of the sample: $\phi = 1 - \frac{\rho_{bd}}{\rho_s}$, and the volume fraction of the rock phase is then $(1-\phi)$. The dielectric constant of air is $\epsilon_{air} = 1$, and the dielectric constant of aluminum oxide and dunite has been found in the literature to be within the range $\epsilon_{Al_2O_3} \approx 9-10$ and $\epsilon_{Dunite} \approx 6-6.6$ respectively (Hickson et al., 2017; von Hippel, 1954; Gershon et al., 2001; Rajab et al., 2008; Tuhkala et al., 2013; Campbell and Ulrichs, 1969; St. Amant, 1968). Several two-phase mixing equations are considered in this study and will be briefly introduced.

The Maxwell-Garnett (MG) formula is one of the oldest and most widely used mixing formulas and assumes spherical inclusions of dielectric constant ϵ_2 randomly embedded in some continuous matrix of dielectric constant ϵ_1 (Maxwell Garnett, 1904; Sihvola, 1999):

$$\epsilon_{eff} = \epsilon_1 + 3f\epsilon_1 \frac{\epsilon_2 - \epsilon_1}{\epsilon_2 + 2\epsilon_1 - f(\epsilon_2 - \epsilon_1)} \tag{4}$$

Here, f refers to the volume fraction of inclusions (and hereafter will correspond to the phase with ϵ_2). Inherent in the MG formula is the asymmetry with respect to which phase of the mixture is considered the inclusion or matrix phase, and the assumption that the inclusions are far apart such that their induced electric fields do not significantly affect the polarizability of any one inclusion (Sihvola, 1999; Jylhä, 2008). At low volume fractions of inclusions this latter assumption is satisfied; however, at higher volume fractions the MG formula will tend to underestimate ϵ_{eff}. The Inverse Maxwell-Garnett (IMG) formula refers to the MG formula with the mixture phases flipped from some original definition: $\epsilon_{1,\,MG} \rightarrow \epsilon_{2,\,IMG}$ and $\epsilon_{2,\,MG} \rightarrow \epsilon_{1,\,IMG}$.

The Bruggeman Symmetric (BS) formula is similar to the MG formula in that it assumes spherical inclusions embedded in a matrix; however, the phases are treated as separate inclusions with dielectric constants ϵ_1 and ϵ_2 (for a two phase mixture), and the dielectric constant of the matrix takes on the effective dielectric constant of the overall mixture (Bruggeman, 1935; Sihvola, 1999):

$$(1-f)\frac{\epsilon_1 - \epsilon_{eff}}{\epsilon_1 + 2\epsilon_{eff}} + f\frac{\epsilon_2 - \epsilon_{eff}}{\epsilon_2 + 2\epsilon_{eff}} = 0 \tag{5}$$

Unlike the MG formula, the BS formula is symmetric with respect to the phases of the mixture and is valid for a wider range of volume fractions of each mixture phase.

The Looyenga–Landau–Lifshitz (LLL) formula was derived from differential analysis independently by Landau and Lifshitz (1960) and Looyenga (1965), for which the model assumes a homogeneous mixture and is independent of particle shape:

$$\epsilon_{eff}^{\frac{1}{3}} = f\epsilon_2^{\frac{1}{3}} + (1-f)\epsilon_1^{\frac{1}{3}} \tag{6}$$

The LLL formula is symmetric with respect to the phases of the mixture, but does not not consider the polarizability of single particles in its derivation and is not as suitable as the MG or BS formulas for small volume fractions of either phase for a two phase mixture.

The Lichtenecker (LI) formula, as introduced earlier, was first proposed by Lichtenecker (1926) and has since been derived through differential analysis from several authors in different ways, and in general the model assumes randomly oriented inclusions with arbitrary shapes (Lichtenecker, 1926; Sihvola, 1999; Goncharenko et al., 2000; Simpkin, 2010):

$$\epsilon_{eff} = \epsilon_2^f \epsilon_1^{1-f} \tag{7}$$

The LI formula is symmetric with respect to the phases of the mixture and averages the logarithms of ϵ_1 and ϵ_2.

4.2. Modeling experimental results

To determine which mixing model matches our experimental results best, we perform unweighted non-linear least squares regression for each mixing formula introduced in Section 4.1 to find the optimal value for the dielectric constant of aluminum oxide and dunite for each set of measurements, and then compare that value to those found in the literature. The regression was carried out in Python using LMFIT, which uses the Levenberg–Marquardt method for finding the optimal solution for the dielectric constant of the sample material (Newville et al., 2014). In a previous work we showed that boundary effects in the coaxial airline can significantly affect the measured dielectric constant, and thus we also apply the boundary effect correction (Hickson et al., 2017). The result of the regression analysis is given for the aluminum oxide samples in Table 3 and the dunite samples in Table 4.

The mixing equations that fit the data with a dielectric constant closest to those found in the literature for aluminum oxide and dunite were the Bruggeman Symmetric (BS) and Looyenga–Landau–Lifshitz (LLL) equations. The Maxwell-Garnett (MG) and Inverse Maxwell-Garnett (IMG) equations did not produce realistic results, which is expected since the porosity (volume fraction of air) of all the measurements considered was in the range $\phi \approx 0.4 - 0.6$ (40–60% air). Interestingly the value for the dielectric constant that provided the best fit for the Lichtenecker (LI) equation was significantly larger than that found in the literature, indicating that the LI model underestimates the effective dielectric constant for a given mixture. These trends are consistent with several other studies in the literature investigating the accuracy of these mixing formulas (Tuhkala et al., 2013; Nelson, 1992; Hickson et al., 2017; St. Amant, 1968; Nelson and Bartley, 1998; Tuncer, 2010; Scheller et al., 2010; Dube, 1970). The simple form of the LLL equation compared to the BS equation and its generality relative to assumptions on particle shape make it an ideal model for planetary regolith, for which a range of irregular particle shapes could be present. The LLL formula can be rewritten to represent regolith (and the powder measurements in this study) as a function of only the bulk density, ρ_{bd}, similar to Eq. (2):

$$\epsilon_{eff} = (\rho_{bd}\alpha + 1)^3, \quad where\ \alpha = \frac{1}{\rho_s}(\epsilon_s^{1/3} - 1) \tag{8}$$

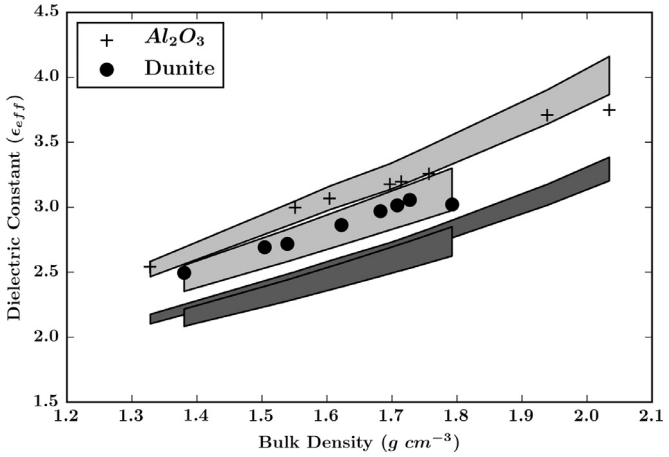

Fig. 3. Measurements of the effective dielectric constant of aluminum oxide and dunite powders (Table 2). The region shaded light grey is the theoretical range in the effective dielectric constant by the LLL model (for both aluminum oxide [$\epsilon_{Al_2O_3} = 9 - 10$, upper] and dunite [$\epsilon_{dunite} = 6 - 7$, lower]). The region shaded dark grey is the theoretical range in the effective dielectric constant by the LI model (for both aluminum oxide [$\epsilon_{Al_2O_3} = 9 - 10$, upper] and dunite [$\epsilon_{dunite} = 6 - 7$, lower]). All mixing equation calculations are made with boundary effects corrected as outlined in Hickson et al. (2017) in order to match experimental data. The dark grey regions corresponding to the LI model plot below the measured data.

Eq. (8) represents a two phase mixture of solid rock grains and void spaces ($\epsilon_{air} = 1$) according to the LLL mixing model. In Eq. (8), the effective dielectric constant of the powder is dependent on the bulk density, ρ_{bd}, and a constant, α, that is determined by the solid density, ρ_s, and solid dielectric constant, ϵ_s, of the powder material. This is similar to the dependence of Eq. (2) on ρ_{bd} and a, which is also a function of ρ_s and ϵ_s. The solid density of the aluminum oxide and dunite samples used in this study was presented in Section 2.2: $\rho_{Al_2O_3} = 3.8\,\mathrm{g/cm^3}$ and $\rho_{dunite} = 3.29 \pm 0.06\,\mathrm{g/cm^3}$. Using a conservative range of values for the dielectric constant of both aluminum oxide ($\epsilon_{Al_2O_3} = 9 - 10$) and dunite ($\epsilon_{dunite} = 6 - 7$) found in the literature, we can calculate the *theoretical range* in the effective dielectric constant as a function of bulk density that corresponds to both the LI model (Eq. (2)) and the LLL model (Eq. (8)). The experimental results from this study are plotted with the theoretical range in the effective dielectric constant with bulk density (with boundary effects considered) for both aluminum oxide and dunite in Fig. 3.

Consistent with the results shown in Tables 3, 4 and Fig. 3, the LI model underestimates the effective dielectric constant of powder mixtures for the appropriate solid dielectric constant and solid density of the material. The LLL model calculates an effective dielectric constant consistent with the powder sample measurements presented in this study. It should be noted that the shaded regions in Fig. 3 are not regression fits, but the results of applying the LLL and LI mixing models with boundary effects corrected for each corresponding measurement, with the range in solid dielectric constants for aluminum oxide and dunite from the literature used to bound each region. An important result from this analysis is that the particle density, in addition to the solid dielectric constant of powder grains, contributes to the mixing model results.

The LI equation was first used by Olhoeft and Strangway (1975) to model permittivity measurements of Lunar regolith samples brought back from NASA's Apollo missions. We further compare the LLL and LI models by fitting each to the permittivity measurements of Lunar regolith presented in Carrier et al. (1991). The same regression procedure is used to find the optimal value of a in Eq. (2) (LI) and of α in Eq. (8) (LLL). The data chosen for our analysis are the permittivity measurements from Carrier et al. (1991) that were conducted in vacuum; for a com-

Table 2
Aluminum oxide and dunite powder sample measurements. Note the first aluminum oxide measurement was not measured in vacuum and was calibrated using the SOLT method (see (Hickson et al., 2017)) and has a higher standard deviation than the other measurements.

Sample description	Dielectric constant, ϵ_{eff}	Bulk density, ρ_{bd}, (g/cm^3)	Avg. grain size (μm)
Aluminum oxide	3.75 ± 0.09	2.034 ± 0.002	76
Aluminum oxide	3.71 ± 0.04	1.939 ± 0.002	102
Aluminum oxide & silica aerogel	3.26 ± 0.04	1.757 ± 0.002	102
Aluminum oxide & silica aerogel	3.20 ± 0.03	1.714 ± 0.002	102
Aluminum oxide & silica aerogel	3.18 ± 0.03	1.697 ± 0.002	102
Aluminum oxide & silica aerogel	3.07 ± 0.03	1.604 ± 0.002	76
Aluminum oxide & silica aerogel	3.00 ± 0.03	1.551 ± 0.001	76
Aluminum oxide & silica aerogel	2.54 ± 0.04	1.328 ± 0.001	76
Dunite	3.021 ± 0.007	1.792 ± 0.002	113
Dunite	3.058 ± 0.009	1.727 ± 0.002	113
Dunite	3.017 ± 0.004	1.708 ± 0.002	109
Dunite	2.971 ± 0.003	1.682 ± 0.002	109
Dunite & silica aerogel	2.865 ± 0.006	1.622 ± 0.002	109
Dunite & silica aerogel	2.720 ± 0.006	1.539 ± 0.001	113
Dunite & silica aerogel	2.692 ± 0.004	1.504 ± 0.001	109
Dunite & silica aerogel	2.498 ± 0.004	1.380 ± 0.001	109

Table 3
Two phase mixing model fits for aluminum oxide dielectric constant. Corrected dielectric constant refers to the respective mixing formulas being applied with the boundary effects of the coaxial airline considered as outlined in Hickson et al. (2017). References for values in the literature: Hickson et al. (2017), von Hippel (1954), Gershon et al. (2001), Rajab et al. (2008) and Tuhkala et al. (2013).

Mixing equation	Dielectric constant, ϵ_s	Corrected dielectric constant, $\epsilon_{s,\,corr}$
Maxwell-Garnett (MG)	41.02	55.46
Inverse Maxwell-Garnett (IMG)	7.03	7.37
Bruggeman Symmetric (BS)	8.64	9.01
Looyenga–Landau–Lifshitz (LLL)	8.68	9.12
Lichtenecker (LI)	13.03	13.76
Values in the literature	$\approx 9-10$	$\approx 9-10$

Table 4
Two phase mixing model fits for dunite dielectric constant (same definition as in Table 3 for corrected dielectric constant). The highest bulk density measurement of dunite was considered an outlier and removed from the regression analysis. References for values in the literature: Campbell and Ulrichs (1969) and St. Amant (1968).

Mixing equation	Dielectric constant, ϵ_s	Corrected dielectric constant, $\epsilon_{s,\,corr}$
Maxwell-Garnett (MG)	11.56	12.42
Inverse Maxwell-Garnett (IMG)	5.51	5.68
Bruggeman Symmetric (BS)	6.32	6.53
Looyenga–Landau–Lifshitz (LLL)	6.38	6.59
Lichtenecker (LI)	8.49	8.83
Values in the literature	$\approx 6-6.6$	$\approx 6-6.6$

prehensive list see (Carrier et al., 1991). The data are not cited with any uncertainty in Carrier et al. (1991), and the regression is meant to give a qualitative result. The optimal fit for the LI equation is $\epsilon_{eff} = 1.96^{\rho_{bd}}$ and for the LLL equation is $\epsilon_{eff} = (\rho_{bd} 0.307 + 1)^3$, which is plotted along with the corresponding Lunar regolith permittivity measurements in Fig. 4.

Both the LI and LLL equations have reasonable fits to the Apollo Lunar regolith permittivity measurements with similar root mean square error's (RMSE) of 0.6723 and 0.6930 respectively. The optimal values for the constants a and α have implications for the corresponding solid density and solid dielectric constant of the Lunar regolith samples. The range in composition and mineralogy between the various Apollo mission landing sites implies that the fits for the LI and LLL equations correspond to average Lunar regolith properties. When performing the same regression analysis for Apollo missions 15, 16, and 17 separately, we observe that the

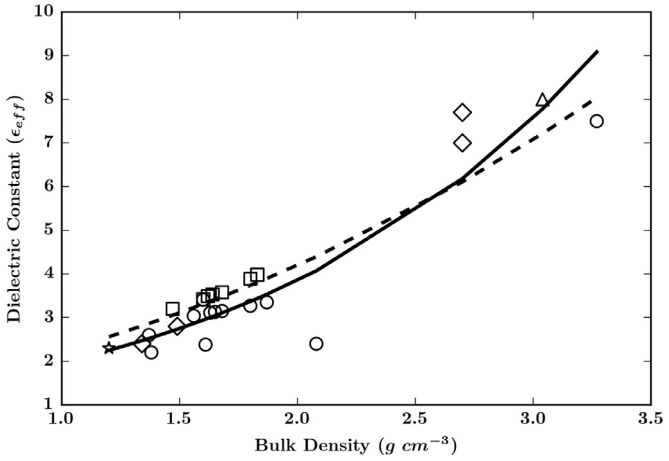

Fig. 4. Regression analysis of Apollo Lunar regolith permittivity measurements from Carrier et al. (1991). Squares are data from Apollo 15, circles from Apollo 17, diamonds from Apollo 16, stars from Apollo 14, and triangles from Apollo 12 (there is only one data point each for Apollo missions 14 and 12). The optimal fit for the LI equation is the solid line, and the optimal fit for the LLL equation is the dotted line.

values of a and α correlate well with average titanium dioxide and iron oxide weight percentages and solid density measurements of regolith samples returned during each mission. This analysis of Lunar regolith permittivity measurements supports the results observed in our experimental data.

5. NEA regolith bulk density modeling

In Section 1.1 the concept of deriving the effective dielectric constant of asteroid regolith from radar reflections was introduced. The relation between the OC geometric radar albedo, $\hat{\sigma}_{OC}$ and Fresnel reflection coefficient, R_f, is often cited as: $\hat{\sigma}_{OC} = gR_f$, where g is the backscatter gain and is dependent on the targets shape and orientation (Ostro et al., 1985; Mitchell et al., 1996; Magri et al., 2001; Evans and Hagfors, 1966). Regardless of which scattering law is chosen for the target, g is on the order of $1 + \frac{1}{2}S_o^2$, where $S_o = \tan(\theta_{r.m.s})$, and $\theta_{r.m.s}$ is the adirectional root-mean-square (r.m.s) slope of the asteroid surface (on the scale of the observing wavelength) (Mitchell et al., 1996; Magri et al., 2001). Ostro et al. (1985) proposed that values of g are generally $g < 1.5$ for any rough-surface scattering law, and that changes in $\hat{\sigma}_{OC}$ between observed asteroids are driven by changes in R_f rather than g. Magri et al. (2001) expanded on the Garvin et al. (1985) model for

estimating asteroid regolith bulk densities from radar reflections, using the following equation to estimate the portion of $\hat{\sigma}_{OC}$ that is due solely to specular reflections, $\hat{\sigma}_{OCqs}$:

$$\hat{\sigma}_{OCqs} = \hat{\sigma}_{OC}\left(1 - \frac{\mu_c}{\mu_{c,diff}}\right) \tag{9}$$

Here $\mu_{c,\,diff}$ is the diffuse circular polarization ratio and μ_c is the circular polarization ratio as defined in Section 1.1. Magri et al. (2001) use $\mu_{c,diff} = 0.50 \pm 0.15$, taken from Harmon and Ostro (1985) as that for the Moon. Making use of this quasi-specular portion of radar reflections from asteroid surfaces, the resulting (uncalibrated) model for asteroid regolith bulk density by Magri et al. (2001) can be written as follows:

$$\rho_{bd} = \left(\frac{2}{ln[a]}\right) ln\left[\frac{1 + \sqrt{\frac{\hat{\sigma_{OC}}}{g}(1 - \frac{\mu_c}{\mu_{c,diff}})}}{1 - \sqrt{\frac{\hat{\sigma_{OC}}}{g}(1 - \frac{\mu_c}{\mu_{c,diff}})}}\right] \tag{10}$$

The first term on the right hand side corresponds to the LI mixing model in the form of Eq. (2). The value of a in Magri et al. (2001) is $a = 1.87$, taken from Garvin et al. (1985) (see Table 1). Magri et al. (2001) use bulk density estimates to calculate porosity and solid density of asteroid regoliths; however, the value of a is dependent on the solid density of the regolith material and is inherently assumed prior to obtaining bulk density estimates. Nolan et al. (2013) used Eq. (10) to model the surface bulk density of (101955) Bennu using Arecibo S- band radar data in support of the OSIRIS-REx mission. Nolan et al. (2013) calculated the bulk density of Bennu to be $\rho_{bd} = 1.65\,\mathrm{g/cm^3}$ within the upper 1 m of the surface.

The results of Section 4 show that the LLL mixing equation matches laboratory permittivity measurements better than the LI mixing equation, and is therefore more appropriate for asteroid regoliths. Eq. (10) can be rewritten to incorporate the LLL mixing model rather than the LI mixing model as follows:

$$\rho_{bd} = \frac{1}{\alpha}\left(\left[\frac{1 + \sqrt{\frac{\hat{\sigma_{OC}}}{g}(1 - \frac{\mu_c}{\mu_{c,diff}})}}{1 - \sqrt{\frac{\hat{\sigma_{OC}}}{g}(1 - \frac{\mu_c}{\mu_{c,diff}})}}\right]^{2/3} - 1\right) \tag{11}$$

From the experimental results of Section 4.2, given appropriate estimates of α, Eq. (11) will provide more accurate estimates of asteroid regolith bulk density within the radar penetration depth than Eq. (10). As was shown in Section 4.2, $\alpha = \frac{1}{\rho_s}(\epsilon_s^{1/3} - 1)$ and depends on the solid density, ρ_s, and solid dielectric constant, ϵ_s, of the asteroid regolith material. Lauretta et al. (2015) summarize the spectral designation of Bennu as a B- type asteroid with possible meteorite analogues to be CI or CM carbonaceous chondrites. Consolmagno et al. (2008) give CI chondrite average grain (solid) density as $\rho_s = 2.46 \pm 0.04\,\mathrm{g/cm^3}$ and CM chondrite average grain density as $\rho_s = 2.90 \pm 0.08\,\mathrm{g/cm^3}$. The exact composition and solid dielectric constant of the regolith material on Bennu is uncertain, so we consider the range $\epsilon_s = (5.0 \pm 0.5) - (8.0 \pm 0.5)$ for analysis, which spans most of the measurements of Campbell and Ulrichs (1969) for geologic materials. Using these ranges for solid density and solid dielectric constant, along with the values $g = 1.2 \pm 0.1$ corresponding to r.m.s slope of $\approx$\30° and $\mu_{c,diff} = 0.50 \pm 0.15$ from Magri et al. (2001), new estimates for the bulk density of the regolith on Bennu are given in Table 5. The radar data used for the estimates in Table 5 are taken from Nolan et al. (2013): $\hat{\sigma}_{OC} = 0.12 \pm 0.04$ and $\mu_c = 0.18 \pm 0.03$.

The values in Table 5 show that when considering spectral analogues as proxies for the composition on Bennu and using the more appropriate LLL mixing model, the estimated bulk density in the near surface is generally lower than that given by Nolan et al. (2013). Assuming average material properties of $\rho_s = 2.68 \pm 0.09\,\mathrm{g/cm^3}$ and $\epsilon_s = 6.5 \pm 0.71$ for the regolith on Bennu, Eq. (11) calculates an average bulk density for the near surface of $\rho_{bd} = 1.27 \pm 0.33\,\mathrm{g/cm^3}$. At the associated solid density of $\rho_s = 2.68 \pm 0.09\,\mathrm{g/cm^3}$, this corresponds with a macroporosity, ϕ, of $\phi = 0.52 \pm 0.12$ (or 52% void space). The new estimates for average bulk density and macroporosity given in this study are in agreement with those by Chesley et al. (2014) of $\rho_{bd} = 1.26 \pm 0.07\,\mathrm{g/cm^3}$ and $\phi = 0.40 \pm 10$ derived using radar astrometry combined with infrared astronomy and Yarkovsky effect modeling.

Table 5
Bulk density values using Eq. (11) for the near surface of Bennu.

	$\rho_s = 2.46 \pm 0.04\,\mathrm{g/cm^3}$	$\rho_s = 2.90 \pm 0.08\,\mathrm{g/cm^3}$
$\epsilon_s = \mathbf{5 \pm 0.5}$	$\rho_{bd} = 1.43 \pm 0.37\,\mathrm{g/cm^3}$	$\rho_{bd} = 1.68 \pm 0.43\,\mathrm{g/cm^3}$
$\epsilon_s = \mathbf{8 \pm 0.5}$	$\rho_{bd} = 1.01 \pm 0.25\,\mathrm{g/cm^3}$	$\rho_{bd} = 1.19 \pm 0.30\,\mathrm{g/cm^3}$

Radar observations of (162173) Ryugu to estimate the near surface bulk density in anticipation of the Hayabusa2 sample return mission are currently not available. Ostro et al. (2004) observed (25143) Itokawa during its 2001 close approach using Arecibo and Goldstone observatories and obtained average values of $\hat{\sigma_{OC}} = 0.16 \pm 0.05$ and $\mu_c = 0.26 \pm 0.04$. Using the original model from Magri et al. (2001) the near surface bulk density was estimated to be $\rho_{bd} = 1.66\ (+0.35 - 0.65)\,\mathrm{g/cm^3}$. The composition of Itokawa is similar to LL ordinary chondrites, for which the average grain (solid) density according to Consolmagno et al. (2008) is $\rho_s = 3.54 \pm 0.13\,\mathrm{g/cm^3}$. Using this solid density value and the range for solid dielectric constant $\epsilon_s = 5.0 \pm 0.5 - 8.0 \pm 0.5$ we calculate the range in possible near surface bulk density on Itokawa to be $\rho_{bd} = 1.46 \pm 0.45 \rightarrow 2.05 \pm 0.64\,\mathrm{g/cm^3}$, with an average of $\rho_{bd} = 1.68 \pm 0.53\,\mathrm{g/cm^3}$ corresponding to a macroporosity of $\phi = 0.53 \pm 0.15$. This is in agreement with the bulk density of $\rho_{bd} = 1.9 \pm 0.13\,\mathrm{g/cm^3}$ determined by analysis of data returned during the Hayabusa mission (Fujiwara et al., 2006).

6. Conclusion

New estimates for the average bulk density $\rho_{bd} = 1.27 \pm 0.33\,\mathrm{g/cm^3}$ and porosity $\phi = 0.52 \pm 0.12$ in the near surface of (101955) Bennu have been been derived from radar data using an updated mixing model with experimental validation. Measurements of the dielectric constant of aluminum oxide and dunite powders in low vacuum were used to show the Looyenga–Landau–Lifshitz (LLL) mixing model is more appropriate than the Lichtenecker (LI) model, which has typically been used to approximate planetary regolith. The LLL model was shown to agree well with permittivity measurements of Lunar regolith, and the dependence of both the LLL and LI model on composition and mineralogy was highlighted. Silica aerogel was used for the first time to vary the bulk density of the sample powders without significantly altering the electrical properties. This process can be applied to any geologic powder permittivity measurements, for which future measurements of a wider variety of materials at different densities will help to further constrain possible mixing models. The model used to calculate asteroid regolith bulk density is an updated version of that presented in Magri et al. (2001), with the LLL mixing model used instead of the LI model. The significant error in the bulk density estimates of asteroid regoliths arises from the many modeling assumptions; however, within one standard deviation the average bulk density estimate for Bennu is lower than that given by Nolan et al. (2013) which used the original model in Magri et al. (2001). A bulk density in the near surface regolith of Bennu of $\rho_{bd} = 1.27 \pm 0.33\,\mathrm{g/cm^3}$ implies that the near surface density is similar to the bulk density calculated by Chesley et al. (2014). In this study the asteroid regolith bulk den-

sity is derived taking into consideration the probable solid density of the regolith material. In this way, estimates of porosity are more reliable than previous estimates that used mixing models with assumed values of solid particle density with no relation to the specific asteroid.

A future consideration for inversely solving for asteroid surface properties from radar data is the presence of water and other volatiles, which is especially important for C- type asteroids. This is also significant for the study of comet nuclei, which are similar to C- type asteroids. Permittivity measurements of rock and ice mixtures are necessary to see if the LLL model is also suitable for water phases, i.e (Brouet et al., 2016). Similar work can also be applied to Mars radar sounding studies such as (Watters et al., 2017), where laboratory permittivity measurements of Martian regolith analogue minerals are needed to extend the applicability of the LLL mixing equation to other planetary surfaces. In Eq. (11) material estimates of solid density and solid dielectric constant provide additional constraints to modeling. We propose the use of Eq. (11) from this study as a replacement to the model proposed by Magri et al. (2001) (Eq. (10)).

The inherent scattering assumptions in estimating Fresnel reflectivity from asteroid radar data using the approach of Magri et al. (2001) introduce large uncertainty to regolith bulk density calculations in this study and inhibit the ability to draw solid conclusions about regolith properties. The assumptions in handling diffuse and multiple scattering imply that this approach is better suited for asteroids with low μ_c. Describing this scattering behavior of the regolith simply by estimates of a backscatter gain and diffuse circular polarization ratio introduce large sources of uncertainty to the asteroid radar model. Furthermore, it has been shown that subsurface rocks embedded in the regolith can enhance radar echoes, and that surface scatterers likely play a significant role in contributing to radar echoes of NEAs (Benner et al., 2008; Virkki and Muinonen, 2016). Future asteroid radar modeling efforts, such as (Virkki et al., 2017), should explore incorporating the Looyenga–Landau–Lifshitz mixing model for more robust calculations of regolith bulk density.

Acknowledgments

This work was funded by the Canadian Space Agency (CSA) and the Natural Sciences and Engineering Research Council of Canada (NSERC).

Supplementary material

Supplementary material associated with this article can be found, in the online version, at 10.1016/j.icarus.2018.01.018.

References

Barmatz, M., Steinfeld, D., Winterhalter, D., Rickman, D., Gustafson, R., Butts, D., Weinstein, M., 2012. Microwave permittivity and permeability measurements on lunar simulants. 43rd Lunar and Planetary Science Conference Abstract 1050.. Abstract 1050

Benner, L., Busch, M., Giorgini, J., Taylor, P., Margot, J., 2015. Radar observations of near-earth and main-belt asteroids. Asteroids IV 1, 165–182. doi:10.2458/azu_uapress_9780816532131-ch009.

Benner, L., Ostro, S., Magri, C., Nolan, M., Howell, E., Giorgini, J., Jurgens, R., Margot, J., Taylor, P., Busch, M., Shepard, M., 2008. Near-earth asteroid surface roughness depends on compositional class. Icarus 198 (2), 294–304. doi:10.1016/j.icarus.2008.06.010.

Binzel, R., Harris, A., Bus, S., Burbine, T., 2001. Spectral properties of near-earth objects: palomar and IRTF results for 48 objects including spacecraft targets (9969) Braille and (10302) 1989 ml. Icarus 151, 139–149. doi:10.1006/icar.2001.6613.

Boughriet, A.-H., Legrand, C., Chapoton, A., 1997. Noniterative stable transmission/reflection method for low-loss material complex permittivity determination. IEEE Trans. Microw. Theory Tech. 45 (1), 52–57. doi:10.1109/22.552032.

Britt, D.T., Yeomans, D., Housen, K., Consolmagno, G., 2002. Asteroid density, porosity, and structure. In: Bottke, W.F., Cellino, A., Paolicchi, P., Binzel, R.P. (Eds.). In: Asteroids III. Univ. of Arizona Press, Tucson, pp. 485–500.

Brouet, Y., Neves, L., Sabouroux, P., Levasseur-Regourd, A., Poch, O., Encrenaz, P., Pommerol, A., Thomas, N., Kofman, W., 2016. Characterization of the permittivity of controlled porous water ice-dust mixtures to support the radar exploration of icy bodies. J. Geophys. Res. Planets 121 (12), 2426–2443. doi:10.1002/2016JE005045.

Bruggeman, V.D., 1935. Berechnung cershiedener physikalisher konstanten von heterogenen substanzen. i. dielektrizitätskonstanten und leitfähigkeiten der mischkörper aus isotropen substanzen. Ann. Phys. 416 (7), 636–664. doi:10.1002/andp.19354160705.

Bus, S., Binzel, R., 2002. Phase II of the small main-belt asteroid spectroscopic survey: a feature-based taxonomy. Icarus 158 (1), 146–177. doi:10.1006/icar.2002.6856.

Bussey, H., 1979. Microwave dielectric measurements of lunar soil with a coaxial line resonator method. Proceedings of the 10th Conference on Lunar and Planetary Science 3, 2175–2182.

Campbell, B., 2002. Radar Remote Sensing of Planetary Surfaces. Cambridge University Press.

Campbell, B.A., 2016. Planetary geology with imaging radar: insights from earth-based lunar studies, 2001–2015. Publ. Astron. Soc. Pac. 128 (964), 1–20. doi:10.1088/1538-3873/128/964/062001.

Campbell, M., Ulrichs, J., 1969. Electrical properties of rocks and their significance for lunar radar observations. J. Geophys. Res. 74 (25), 5867–5881. doi:10.1029/JB074i025p05867.

Carrier, W., Olhoeft, G., Mendell, W., 1991. Physical properties of the lunar surface. Lunar sourcebook 475–594.

Carter, L., Campbell, D., Campbell, B., 2011. Geologic studies of planetary surfaces using radar polarimetric imaging. Proc. IEEE 99 (5), 770–782. doi:10.1109/JPROC.2010.2099090.

Chesley, S., Farnocchia, D., Nolan, M., Vokrouhlickỳ, D., Chodas, P., Milani, A., Spoto, F., Rozitis, B., Benner, L., Bottke, W., Busch, M., Emery, J., Howell, E., Lauretta, D., Margot, J., Taylor, P., 2014. Orbit and bulk density of the OSIRIS-REx target Asteroid (101955) Bennu. Icarus 235, 5–22. doi:10.1016/j.icarus.2014.02.020.

Clark, B., Binzel, R., Howell, E., Cloutis, E., Ockert-Bell, M., Christensen, P., Barucci, M., DeMeo, F., Lauretta, D., Connolly, H., Soderberg, A., Hergenrother, C., Lim, L., Emery, J., Mueller, M., 2011. Asteroid (101955) 1999 RQ36: spectroscopy from 0.4 to 2.4 μm and meteorite analogs. Icarus 216, 462–475. doi:10.1016/j.icarus.2011.08.021.

Clark, B., Hapke, B., Pieters, C., Britt, D., 2002. Asteroid space weathering and regolith evolution. In: Bottke, W.F., Cellino, A., Paolicchi, P., Binzel, R.P. (Eds.). In: Asteroids III. Univ. of Arizona Press, Tucson, pp. 585–599.

Consolmagno, G., Britt, D., Macke, R., 2008. The significance of meteorite density and porosity. Chemie der Erde Geochem. 68 (1), 1–29. doi:10.1016/j.chemer.2008.01.003.

DeMeo, F., Binzel, R., Slivan, S., Bus, S., 2009. An extension of the bus asteroid taxonomy into the near-infrared. Icarus 202 (1), 160–180. doi:10.1016/j.icarus.2009.02.005.

Dorcheh, A.S., Abbasi, M., 2008. Silica aerogel; synthesis, properties and characterization. J. Mater. Process. Technol. 199 (1), 10–26. doi:10.1016/j.jmatprotec.2007.10.060.

Dube, D., 1970. Study of Landau–Lifhitz–Looyenga's formula for dielectric correlation between powder and bulk. J. Phys. D Appl. Phys. 3 (11), 1648–1652.

Evans, J., Hagfors, T., 1966. Study of radio echoes from the moon at 23 centimeters wavelength. J. Geophys. Res. 71 (20), 4871–4889. doi:10.1029/JZ071i020p04871.

Fujiwara, A., Kawaguchi, J., Yeomans, D., Abe, M., Mukai, T., Okada, T., Saito, J., Yano, H., Yoshikawa, M., Scheeres, D., Barnouin-Jha, O., Cheng, A., Demura, H., Gaskell, R., Hirata, N., Ikeda, H., Kominato, T., Miyamoto, H., Nakamura, A., Nakamura, R., Sasaki, S., Uesugi, K., 2006. The rubble-pile asteroid Itokawa as observed by Hayabusa. Science 312 (5778), 1330–1334. doi:10.1126/science.1125841.

Garvin, J., Head, J., Pettengill, G., Zisk, S., 1985. Venus global radar reflectivity and correlations with elevation. J. Geophys. Res. 90, 6859–6871. doi:10.1029/JB090iB08p06859.

Gershon, D., Calame, J., Birnboim, A., 2001. Complex permittivity measurements and mixing laws of porous alumina. J. Appl. Phys. 89 (12), 8117–8120. doi:10.1063/1.1369401.

Goncharenko, A., Lozovski, V., Venger, E., 2000. Lichtenecker'S equation: applicability and limitations. Opt. Commun. 174 (1), 19–32. doi:10.1016/S0030-4018(99)00695-1.

Gurav, J., Jung, I.-K., Park, H.-H., Kang, E., Nadargi, D., 2010. Silica aerogel: synthesis and applications. J. Nanomater. 2010, 11pp. doi:10.1155/2010/409310.

Harmon, J.K., Nolan, M.C., Ostro, S.J., Campbell, D.B., 2004. Radar studies of comet nuclei and grain comae. In: Festou, M.C., Keller, K.U., Weaver, H.A. (Eds.). In: Comets II. Univ. of Arizona Press, Tucson, pp. 265–279.

Harmon, J., Ostro, S., 1985. Mars: dual-polarization radar observations with extended coverage. Icarus 62 (1), 110–128. doi:10.1016/0019-1035(85)90175-7.

Hickson, D., Sotodeh, S., Daly, M., Ghent, R., Nolan, M., 2017. Improvements on effective permittivity measurements of powdered alumina: implications for bulk permittivity properties of asteroid regoliths. Adv. Space Res. 59 (1), 472–482. doi:10.1016/j.asr.2016.08.011.

von Hippel, A., 1954. Dielectric Materials and Applications. Technology Press of M.I.T. and John Wiley and Sons.

Hrubesh, L., Pekala, R., 1994. Dielectric properties and electronic applications of aerogels. In: Sol-Gel Processing and Applications, pp. 363–367. doi:10.1007/978-1-4615-2570-7_31.

Jylhä, L., 2008. Modeling of electrical properties of composites. Helsinki University of Technology.

KeysightTechnologies, 2014. Applying Error Correction to Network Analyzer Measurements. Keysight Technologies. USA. Literature Number: 5965-7709E.
Landau, L., Lifshitz, E., 1960. Electrodynamics of Continuous Media. Oxford Pergamon Press.
Lauretta, D., Balram-Knutson, S., Beshore, E., Boynton, W., d'Aubigny, C.D., DellaGiustina, D., Enos, H., Gholish, D., Hergenrother, C., Howell, E., Johnson, C., Morton, E., Nolan, M., Rizk, B., Roper, H., Bartels, A., Bos, B., Dworkin, J., Highsmith, D., Lorenz, D., Lim, L., Mink, R., Moreau, M., Nuth, J., Reuter, D., Simon, A., Bierhaus, E., Bryan, B., Ballouz, R., Barnouin, O., Binzel, R., Bottke, W., Hamilton, V., Walsh, K., Chesley, S., Christensen, P., Clark, B., Connolly, H., Crombie, M., Daly, M., Emery, J., McCoy, T., McMahon, J., Scheeres, D., Messenger, S., Nakamura-Messenger, K., Righter, K., Sandford, S., 2017. OSIRIS-REx: sample return from asteroid (101955) Bennu. Space Sci. Rev. 212, 925.
Lauretta, D., Bartels, A., Barucci, M., Bierhaus, E., Binzel, R., Bottke, W., Campins, H., Chesley, S., Clark, B., Clark, B., Cloutis, E., Connolly, H., Crombie, M., Delbo, M., Dworkin, J., Emery, J., Glavin, D., Hamilton, V., Hergenrother, C., Johnson, C., Keller, L., Michel, P., Nolan, M., Sandford, S., Scheeres, D., Simon, A., Sutter, B., Vokrouhlicky, D., Walsh, K., 2015. The OSIRIS-REx target asteroid (101955) Bennu: constraints on its physical, geological, and dynamical nature from astronomical observations. Meteorit. Planet. Sci. 50 (4), 834–849. doi:10.1111/maps.12353.
Lichtenecker, K., 1926. Die dielektrizitätskonstante natürlicher und künstlicher mischkörper. Physikalische Zeitschrift 27 (4), 115–158.
Looyenga, H., 1965. Dielectric constants of heterogeneous mixtures. Physica 31 (3), 401–406. doi:10.1016/0031-8914(65)90045-5.
Magri, C., Consolmagno, G., Ostrch, S., Benner, L., Beeney, B., 2001. Radar constraints on asteroid regolith properties using 433 eros as ground truth. Meteorit. Planet. Sci. 36 (12), 1697–1709. doi:10.1111/j.1945-5100.2001.tb01857.x.
Maxwell Garnett, J., 1904. Colours in metal glasses and in metallic films. Trans. R. Soc. Lond. 203, 385–420.
McKay, D., Heiken, G., Basu, A., Blanford, G., Simon, S., Reedy, R., French, B., Papike, J., 1991. The lunar regolith. Lunar sourcebook 285–356.
Mitchell, D., Ostro, S., Hudson, R., Rosema, K., Campbell, D., Velez, R., Chandler, J., Shapiro, I., Giorgini, J., Yeomans, D., 1996. Radar observations of asteroids 1 Ceres, 2 Pallas, and 4 Vesta. Icarus 124, 113–133. doi:10.1006/icar.1996.0193.
Nelson, S., 1992. Estimation of permittivities of solids from measurements on pulverized or granular materials. Dielectr. Prop. Heterog. Mater. Progr. Electromagn. Res. 6, 231–271.
Nelson, S., Bartley, P., 1998. Open-ended coaxial-line permittivity measurements on pulverized materials. IEEE Trans. Instrum. Meas. 47 (1), 133–137. doi:10.1109/19.728805.
Newville, M., Ingargiola, A., Stensitzki, T., Allen, D., 2014. Lmfit: non-linear least-square minimization and curve-fitting for python. Zenodo doi:10.5281/zenodo.11813.
Nolan, M., Magri, C., Howell, E., Benner, L., Giorgini, J., Hergenrother, C., Hudson, R., Lauretta, D., Margot, J., Ostro, S., Scheeres, D., 2013. Shape model and surface properties of the OSIRIS-REx target asteroid (101955) Bennu from radar and lightcurve observations. Icarus 226 (1), 629–640. doi:10.1016/j.icarus.2013.05.028.
Olhoeft, G., Strangway, D., 1975. Dielectric properties of the first 100 meters of the moon. Earth Planet. Sci. Lett. 24 (3), 394–404. doi:10.1016/0012-821X(75)90146-6.
Ostro, S., 1993. Planetary radar astronomy. Rev. Mod. Phys. 65 (4), 1235–1279. doi:10.1103/RevModPhys.65.1235.
Ostro, S., Benner, L., Nolan, M., Magri, C., Giorgini, J., Scheeres, D., Broschart, S., Kaasalainen, M., Vokrouhlickỳ, D., Chesley, S., Margot, J., Jurgens, R., Rose, R., Yeomans, D., Suzuki, S., De Jong, E., 2004. Radar observations of asteroid 25143 Itokawa (1998 sf36). Meteorit. Planet. Sci. 39 (3), 407–424. doi:10.1111/j.1945-5100.2004.tb00102.x.
Ostro, S., Campbell, D., Shapiro, I., 1985. Mainbelt asteroids: dual-polarization radar observations. Science 229 (4712), 442–446. doi:10.1126/science.229.4712.442.
Palmer, E., Heggy, E., Capria, M., Tosi, F., 2015. Dielectric properties of asteroid vesta's surface as constrained by dawn VIR observations. Icarus 262, 93–101. doi:10.1016/j.icarus.2015.08.031.
Rajab, K., Naftaly, M., Linfield, E., Nino, J., Arenas, D., Tanner, D., Mittra, R., Lanagan, M., 2008. Broadband dielectric characterization of aluminum oxide (al2o3). J. Microelectron. Electron. Packag. 5 (1), 101–106. doi:10.4071/1551-4897-5.1.1.
Rytting, D., 2001. Network analyzer accuracy overview. In: Procedings of the 58th ARFTG Conference Digest-Fall, 40, pp. 1–13. doi:10.1109/ARFTG.2001.327486.
Scheller, M., Jansen, C., Koch, M., 2010. Applications of effective medium theories in the terahertz regime. Recent Optical and Photonic Technologies. InTech.
Sihvola, A., 1999. Electromagnetic mixing formulas and applications. Electromagnetic Wave Series, 47. IET.
Simpkin, R., 2010. Derivation of Lichtenecker's logarithmic mixture formula from Maxwell's equations. IEEE Trans. Microw. Theory Tech. 58 (3), 545–550. doi:10.1109/TMTT.2010.2040406.
St. Amant, M., 1968. Frequency and temperature dependence of dielectric properties of some common rocks. Massachusetts Institute of Technology.
Tuhkala, M., Juuti, J., Jantunen, H., 2013. Method to characterize dielectric properties of powdery substances. J. Appl. Phys. 114 (1), 014108–1–014108–8. doi:10.1063/1.4812739.
Tuncer, E., 2010. Geometrical description in binary composites and spectral density representation. Materials (Basel) 3 (1), 585–613. doi:10.3390/ma3010585.
Ulaby, F., Bengal, T., Dobson, M., East, J., Garvin, J., Evans, D., 1990. Microwave dielectric properties of dry rocks. IEEE Trans. Geosci. Remote Sens. 28 (3), 325–336. doi:10.1109/36.54359.
Virkki, A., Muinonen, K., 2016. Radar scattering by planetary surfaces modeled with laboratory-characterized particles. Icarus 269, 38–49. doi:10.1016/j. icarus.2016.01.011.
Virkki, A., Taylor, P., Zambrano-Marin, L., Howell, E., Nolan, M., Lejoly, C., Rivera–Valentin, E., Aponte, B., 2017. Near-surface bulk densities of asteroids derived from dual-polarization radar observations. Eur. Planet. Sci. Congr. 11. (abstract EPSC2017-750).
Watters, T., Leuschen, C., Campbell, B., Morgan, G., Cicchetti, A., Grant, J., Phillips, R., Plaut, J., 2017. Radar sounder evidence of thick, porous sediments in meridiani planum and implications for ice-filled deposits on mars. Geophys. Res. Lett. 44 (18), 9208–9215. doi:10.1002/2017GL074431.
Wollensack, M., Hoffmann, J., Ruefenacht, J., Zeier, M., 2012. VNA tools II: S-parameter uncertainty calculation. In: Proceedings of the 79th Conference on Microwave Measurement (ARFTG). IEEE, pp. 1–5.
Yoshikawa, M., Kawaguchi, J., Fujiwara, A., Tsuchiyama, A., 2015. Hayabusa sample return mission. Asteroids IV 1, 397–418. doi:10.2458/azu_uapress_9780816532131-ch021.
Yoshikawa, M., Watanabe, S., Tsuda, Y., Kuninaka, H., the Hayabusa2 Project Team, 2014. Hayabusa2-the next asteroid sample return mission of Japan. Trans. JSASS Aerosp. Tech. Jpn. 12 (29), 29–33.